

WATER SPLITTING STUDIES IN ALKALINE MEDIUM USING GRAPHITE ELECTRODES MODIFIED WITH TRANSITION METAL OXIDES AND COMPOSITIONS CONTAINING THEM

BOGDAN-OVIDIU TARANU^{a,*}, PAULINA VLAZAN^a, ANDREI RACU^a

ABSTRACT. Present day scientific research is focused on the identification of renewable and clean alternatives to fossil fuels, with hydrogen being a promising energy source that fulfills both requirements. Given this context, the current work investigates the water splitting electrocatalytic properties of two hydrothermally synthesized transition metal oxides: MnO₂ and Fe₃O₄. Electrodes were obtained by modifying graphite substrates with suspensions in ethanol containing the catalytic materials as such or in compositions, and their activity for the O₂ and H₂ evolution reactions (OER and HER) was studied in alkaline medium. Out of the MnO₂-based electrodes, the one modified with the suspension containing 2 mg MnO₂, 1 mg Carbon Black and 10 μL Nafion solution displayed an OER overpotential (η_{O_2}) value, at $i = 10 \text{ mA/cm}^2$, of 0.53 V, while the one manufactured using the suspension with 4 mg MnO₂ and 10 μL Nafion solution showed a HER overpotential (η_{H_2}) of 0.427 V (at $i = -10 \text{ mA/cm}^2$). From the Fe₃O₄-based electrodes, the one modified with the suspension containing 2 mg Fe₃O₄ and 2 mg Carbon Black evidenced the highest catalytic activity for both reactions ($\eta_{O_2} = 0.51 \text{ V}$ and $\eta_{H_2} = 0.43 \text{ V}$).

Keywords: water splitting, oxygen evolution reaction, hydrogen evolution reaction, metal oxide, electrocatalysis

INTRODUCTION

Currently, humanity is witnessing an increase in global energy consumption, global warming and environmental pollution. This situation makes the need to develop sustainable energy sources more important than ever [1]. In the past few years, scientific researchers have been focusing on renewable and clean alternatives to fossil fuels [2], and hydrogen appears to be an ideal fuel, emerging both as a renewable and as a clean energy source [3].

^a National Institute for Research and Development in Electrochemistry and Condensed Matter, Dr. A. Paunescu Podeanu street, No. 144, 300569, Timisoara, Romania.

* Corresponding author: b.taranu84@gmail.com.

Hydrogen is abundant in nature due to its presence in water, and current technologies allow its production through renewable, as well as non-renewable sources [4,5]. From the ways in which hydrogen can be generated, water splitting electrolysis stands out as an efficient route with regard to energy conversion and storage, and the necessary power input for this process can be ensured using renewable sources [2,5]. The two half-cell reactions taking place during water splitting are the anodic oxygen evolution reaction (OER) and the cathodic hydrogen evolution reaction (HER), and an important difference between them is that the HER is easier to catalyze, requiring less energy than the OER [6-8]. In the presence of materials that are catalytically active for the two reactions, the amount of energy required for their unfolding decreases [9,10] and, as a result, the potential values at which they occur in practice become closer to the theoretical ones. The search for materials that possess electrocatalytic properties for the OER and HER has led to the identification of efficient catalysts that are also cheaper than the often used noble metal-based ones [10-12]. In fact, the scientific literature includes studies performed using OER, HER, as well as bifunctional catalysts (materials with catalytic activity for both reactions) [13-18].

The present paper describes a study concerning the obtaining of graphite electrodes modified with MnO_2 , Fe_3O_4 and with compositions containing these materials together with Carbon Black and/or Nafion solution, and the evaluation of their OER and HER electrocatalytic properties in alkaline medium. The scientific literature shows that the two transition metal oxides are catalytically active for the two half-cell reactions involved in water splitting [19-30]. It is important to point out that, even though there are these previously reported studies, many of the electrodes investigated herein were manufactured using quantitative compositions that have not been previously tested in terms of their HER and OER electrocatalytic performance. For example, in a study reported by Zhao *et al.* [24] the water splitting properties of defect-engineered ultrathin MnO_2 nanosheets were compared with those of other electrodes, including of a glassy carbon electrode manufactured using a suspension of 5 mg MnO_2 particles and 20 μL Nafion solution dispersed in 980 μL ethanol.

In another investigation, Pokhrel *et al.* [22] evaluated the OER properties of synthesized manganese oxides utilizing electrodes modified with suspensions containing 5 mg catalyst, 5 mg Carbon Black and 45 μL Nafion solution in 350 μL ethanol. In both examples conductive substrate modification procedures that resemble the ones from the present study were employed. There are however important dissimilarities: in this study a different conductive support was used, modified with compositions based on different quantities of catalytic materials, by themselves or mixed with 10 μL

Nafion solution and/or different quantities of Carbon Black. Such dissimilarities exist between the present investigation and those found in other literature reports that focus on the OER and HER properties of electrodes modified with MnO_2 and Fe_3O_4 . Thus, the experimental results and conclusions shown herein serve to complement the current scientific understanding regarding the water splitting catalytic properties of MnO_2 - and Fe_3O_4 -based electrodes.

RESULTS AND DISCUSSION

A. Electrochemical studies

A.1. OER investigations

In the case of the OER experiments performed on the modified electrodes labeled as shown in **Tables 1** and **2** (introduced in the Experimental section), the polarization curves recorded in 0.1M KOH solution revealed that the most electrocatalytically active Fe_3O_4 -based electrode was $\text{G7}_{\text{Fe}_3\text{O}_4}$, while the highest OER catalytic activity among the MnO_2 -based electrodes was observed for $\text{G13}_{\text{MnO}_2}$. As can be seen in **Figure 1a**, at $i = 10 \text{ mA/cm}^2$ - a current density value at which the OER overpotential (η_{O_2}) value is often determined [12,31,32] - these modified electrodes displayed a higher OER activity than the unmodified graphite sample (G0), and this is true for the higher and lower i values as well. The differences between the three curves are clear and, at the specified current density, the η_{O_2} values are 0.66 V for $\text{G7}_{\text{Fe}_3\text{O}_4}$, 0.57 V for $\text{G13}_{\text{MnO}_2}$ and 0.93 V for G0.

The OER properties of the $\text{G7}_{\text{Fe}_3\text{O}_4}$ and $\text{G13}_{\text{MnO}_2}$ electrodes were further studied in 1M KOH solution and the recorded LSVs are presented in **Figure 1b**. By comparing the polarization curves obtained in this strong alkaline medium with those traced in 0.1M KOH solution it is observed that the increase in KOH concentration resulted in an increased OER catalytic activity for both electrodes. Thus, at $i = 10 \text{ mA/cm}^2$, $\eta_{\text{O}_2} = 0.51 \text{ V}$ for $\text{G7}_{\text{Fe}_3\text{O}_4}$ and 0.53 V for $\text{G13}_{\text{MnO}_2}$.

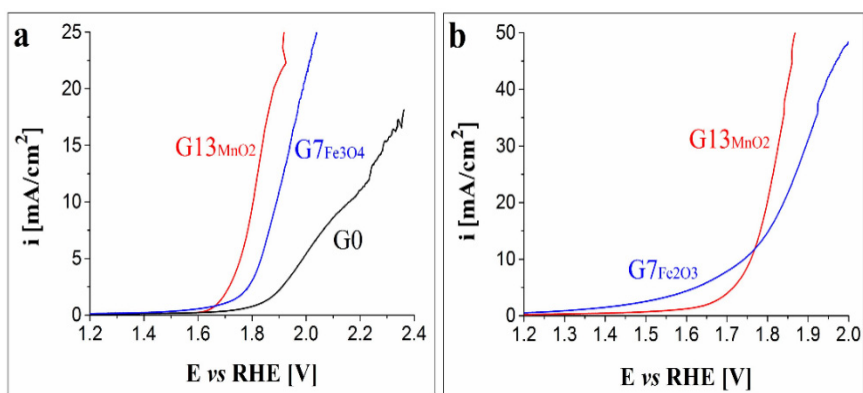


Figure 1. a) LSVs recorded in 0.1M KOH solution on the G0, G7_{Fe3O4} and G13_{MnO2} electrodes. b) LSVs obtained in 1M KOH solution on the G7_{Fe3O4} and G13_{MnO2} electrodes

Because current requirements for materials with OER activity are not limited to the overpotential value, the two modified electrodes were evaluated in terms of other electrochemical characteristics as well. Thus, cyclic voltammetry was employed to estimate their EASA (electroactive surface area) value and the cycles were recorded at different scan rates ($v = 100, 150, 200, 250, 300$ and 350 mV/s), in 1M KNO_3 solution, in the absence and in the presence of 4 mM $\text{K}_3[\text{Fe}(\text{CN})_6]$. Using the acquired data and the Randles-Sevcik equation (presented in the Experimental section), the EASA values were calculated as 0.816 cm^2 for G7_{Fe3O4}, 0.45 cm^2 for G13_{MnO2} and 0.388 cm^2 for G0. Since a higher EASA value is indicative of a higher electrocatalytic activity [33], these results point to the improved catalytic properties of the modified electrodes, compared with the unmodified one. **Figures 2a** and **2b** display the plots of the dependence between the peak current densities of the anodic and cathodic peaks of the ferri-/ferrocyanide redox couple and the square root of the scan rate for G7_{Fe3O4} and G13_{MnO2}, respectively. The results show that the absolute values of the peak current densities increase with the scan rate, which is characteristic of a diffusion-controlled electron transfer process [34].

The OER kinetics at the interface between the modified electrodes and the electrolyte solution were also investigated. **Figure 2c** introduces the Tafel curves for G7_{Fe3O4} and G13_{MnO2}, for which the represented current density values (i_{EASA}) were obtained by taking into account the estimated EASA value. The Tafel slopes were calculated using the Tafel equation [35] and were found to be 0.31 and 0.144 V/dec.

The electrochemical stability of the two modified electrodes was evaluated chronoamperometrically by recording i -time curves (**Figures 3a** and **3b**) during six-hour experiments, at the potential values corresponding to $i = 10 \text{ mA/cm}^2$. In the case of the $\text{G7}_{\text{Fe}_3\text{O}_4}$ electrode the current density did not vary significantly throughout the test. However, the LSVs obtained before and after the investigation (inset in **Figure 3a**) do not overlap entirely. After the test the η_{O_2} values corresponding to low i values increased, while the ones correlated with high i values slightly decreased. Thus, at $i = 10 \text{ mA/cm}^2$ η_{O_2} became 0.55 V. These differences reflect the stability limitations of the studied electrode.

The current density vs. time plot traced during the electrochemical stability test performed on $\text{G13}_{\text{MnO}_2}$ shows that the current density did not vary significantly once it reached 10 mA/cm^2 (at the 98th minute) and that by the end of the experiment it became 9.55 mA/cm^2 . The inset in **Figure 3b** presents the LSVs from before and after the experiment and they evidence some differences in shape that are more pronounced at high current density values. Following the test, the η_{O_2} value at $i = 10 \text{ mA/cm}^2$ slightly changed and became 0.54 V.

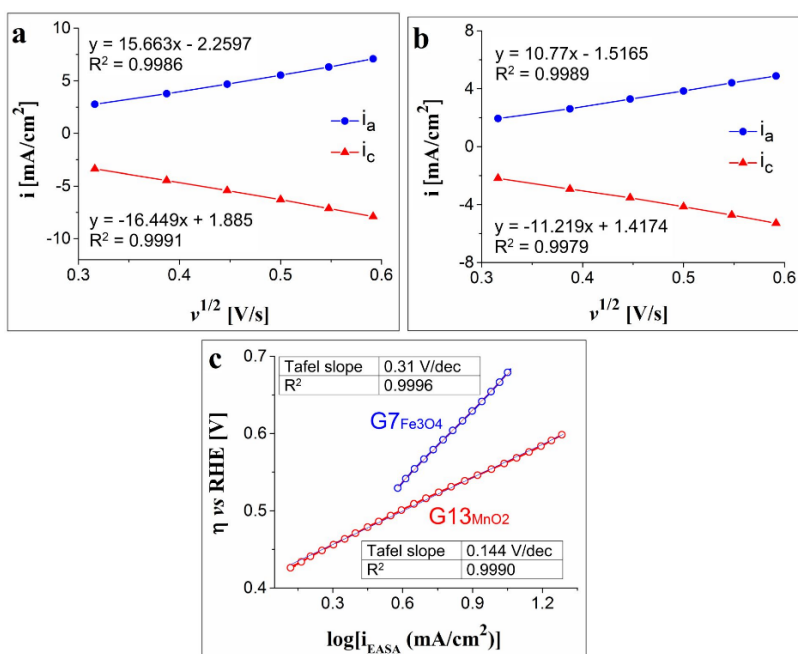


Figure 2. a) The plots of the anodic and cathodic peak current densities vs. the square root of the scan rate (i_a and i_c) for $\text{G7}_{\text{Fe}_3\text{O}_4}$. b) The plots of the anodic and cathodic peak current densities vs. the square root of the scan rate (i_a and i_c) for $\text{G13}_{\text{MnO}_2}$. c) The Tafel plots obtained for $\text{G7}_{\text{Fe}_3\text{O}_4}$ and $\text{G13}_{\text{MnO}_2}$ in 1M KOH solution

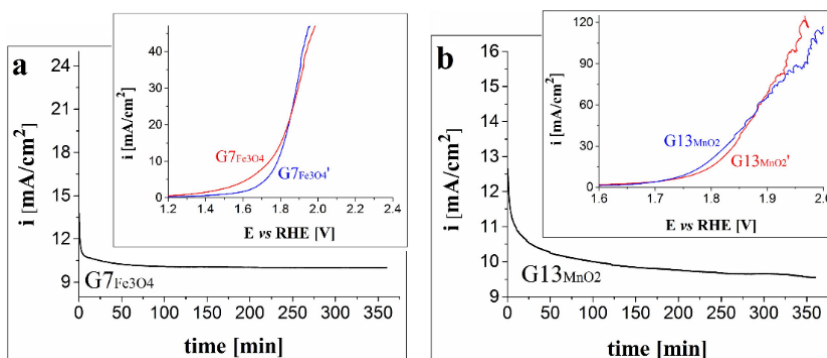


Figure 3. a) The i -time curve obtained on G7_{Fe3O4} in 1M KOH solution and inset with the LSVs from before (G7_{Fe3O4}) and after (G7_{Fe3O4}') the stability test. b) The i -time curve recorded on G13_{MnO2} in 1M KOH solution and inset with the LSVs from before (G13_{MnO2}) and after (G13_{MnO2}') the stability test

A.2. HER investigations

The LSVs recorded in 0.1M KOH solution during the HER investigations performed on the modified electrodes manufactured using the compositions presented in **Tables 1** and **2** allowed for the identification of the most electrocatalytically active samples (**Figure 4a**). Thus, from the Fe₃O₄-based electrodes G7_{Fe3O4} displayed the lowest η_{H_2} value (at $i = -10$ mA/cm²) of 0.52 V. In the case of the MnO₂-modified electrodes, the lowest overpotential value was observed for G11_{MnO2} ($\eta_{H_2} = 0.62$ V). Also, for G0 $\eta_{H_2} = 0.74$ V.

The two electrodes with the highest HER activity were also investigated in strong alkaline medium and the traced cathodic polarization curves are shown in **Figure 4b**. The increase in KOH concentration led to the decrease of the η_{H_2} value – at $i = -10$ mA/cm², η_{H_2} became 0.43 V for G7_{Fe3O4} and 0.427 V for G11_{MnO2}.

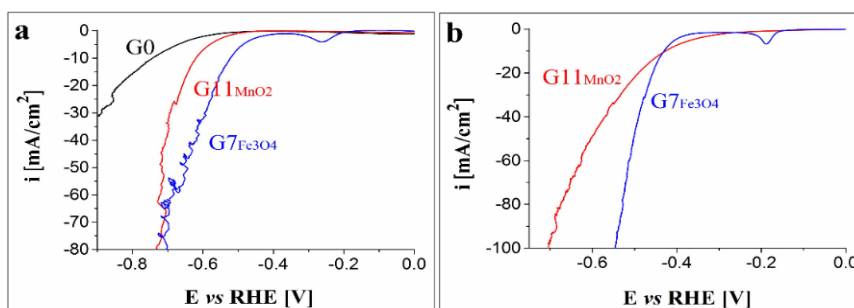


Figure 4. a) LSVs recorded in 0.1M KOH solution on the G0, G7_{Fe3O4} and G11_{MnO2} electrodes. b) LSVs traced in 1M KOH solution on the G7_{Fe3O4} and G11_{MnO2} electrodes

Using the Randles-Sevcik equation and cyclic voltammetry data the EASA value for G11_{MnO2} was estimated as 1.61 cm². The graphical representations of the anodic and cathodic peak current densities vs. the square root of the scan rate for this modified electrode (**Figure 5a**) indicate a diffusion-controlled electron transfer process. The Tafel plots recorded for G7_{Fe3O4} and G11_{MnO2} in 1M KOH solution are presented in **Figures 5b** and **5c**, and the calculated Tafel slope values are 0.117 and 0.213 V/dec, respectively. Since the former value is in the 0.04 ÷ 0.12 V/dec range, it suggests that the HER taking place on the surface of the G7_{Fe3O4} electrode unfolds according to a Volmer-Heyrovsky mechanism, and the charge transfer rate (the discharge step) is controlled by the desorption step [36,37].

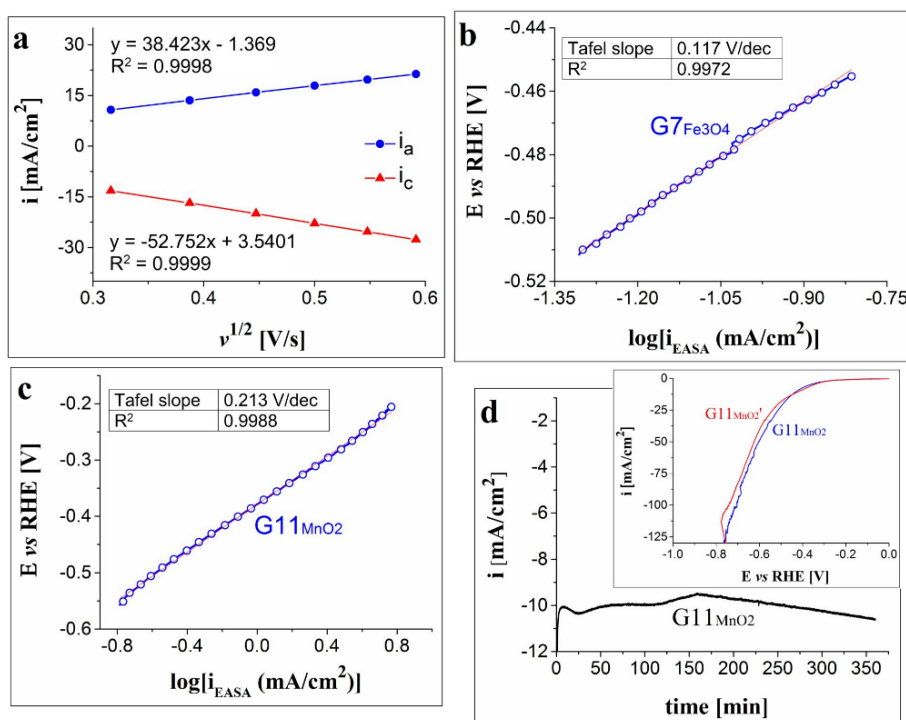


Figure 5. a) The plots of the anodic and cathodic peak current densities vs. the square root of the scan rate (i_a and i_c) for G11_{MnO2}. b) and c) The Tafel plots obtained for G7_{Fe3O4} and G11_{MnO2} in 1M KOH solution. d) The i -time curve recorded on G11_{MnO2} in 1M KOH solution and inset with the LSVs from before (G11_{MnO2}) and after (G11_{MnO2}') the stability test

The electrochemical stability of the electrodes was also investigated. Regrettably, G7_{Fe₃O₄} displayed poor stability and because of this it cannot be used efficiently for the HER in alkaline medium. In the case of G11_{MnO₂}, the chronoamperogram traced during the stability test (**Figure 5d**), by maintaining constant the potential value corresponding to $i = -10 \text{ mA/cm}^2$, evidences the relative stability of the electrode. Thus, the current density value varied around -10 mA/cm^2 throughout the experiment. It increased up to -9.5 mA/cm^2 (160th minute) and subsequently decreased down to -10.6 mA/cm^2 , at the end of the test. The LSVs obtained before and after the study are inserted in **Figure 5d**. Small differences in shape are observed and the η_{H_2} value at -10 mA/cm^2 decreased to 0.414 V – indicating a slight improvement in the catalytic activity of the electrode.

A.3. Further considerations

In general, the OER and HER catalytic activity of a modified electrode is mainly due to structural and transport effects specific to the materials used to modify it [38]. In the case of G7_{Fe₃O₄}, the OER activity was likely the result of the synergistic effect between the materials used to manufacture the electrode – graphite, Fe₃O₄ and Carbon Black - as well as from the quantities of iron oxide and Carbon Black employed to obtain the suspension for substrate modification. The higher the amount of deposited material, the greater the risk that the deposition will organize in the form of thick layers which hinder electrolyte access to the deep pores, leading to a decrease in the electrode's catalytic activity. However, when the deposited amount is too small, the electrode doesn't benefit from enough catalytic material to be efficient. The quantities of 2 mg Fe₃O₄ and 2 mg Carbon Black, utilized to obtain the suspension for the graphite support modification, turned out to be the appropriate amounts amid the ones employed in the present study.

As previously mentioned, the OER catalytic activity of some Fe₃O₄-modified electrodes was investigated by other researchers. For example, Han *et al.* [29] studied the OER on electrodes modified with undoped and Co-doped Fe₃O₄. For the Au electrode modified with undoped Fe₃O₄, the obtained η_{O_2} value, at $i = 10 \text{ mA/cm}^2$ and in strong alkaline medium (1M NaOH), was $\sim 0.59 \text{ V}$. This value is higher than the one outlined for G7_{Fe₃O₄}, at the same current density and in 1M KOH solution. Another example is the analysis reported by Mirabella *et al.* [30], performed on a glassy carbon electrode modified with undoped and Ni-doped Fe₃O₄ (001). The results obtained on the undoped electrode, in 1M NaOH solution, show that the η_{O_2} value is close to 0.6 V even when $i = 4 \text{ mA/cm}^2$. Thus, G7_{Fe₃O₄} is more

catalytically active for the OER than the electrodes manufactured by modifying different conductive substrates with undoped Fe_3O_4 . However, this is no longer the case when considering the doped catalytic materials.

Regarding the HER properties of the $\text{G11}_{\text{MnO}_2}$ electrode, while they probably depend to a large extent on structural and transport effects, a couple of observations are worth being mentioned: 1) the high estimated EASA value for this electrode indicates the presence of surface inhomogeneities that generate additional catalytically active sites and can be in the shape of edges or defects [39,40]; 2) the composition used to modify the electrode doesn't contain Carbon Black - the material that increases the electron transfer between the electrode and the electroactive species. The fact that the electrodes modified with compositions containing Carbon Black did not display a HER catalytic activity as good as that observed for $\text{G11}_{\text{MnO}_2}$ could be related to the formation of thick layers during the modification process. Their presence depends on the way in which the materials from the drop-casted suspensions organize at the surface of the conductive substrates. The thick layers prevent the access of the electrolyte solution to the deep pores [41,42], which leads to a decrease in the HER catalytic performance.

Although the water splitting catalytic activity of the $\text{G11}_{\text{MnO}_2}$ electrode is not superior to that of the MnO_2 -modified electrodes reported in the scientific literature [24,43], the experimental data contributes to increasing the current understanding concerning the water splitting catalytic properties of MnO_2 -based electrodes.

B. Raman analysis

The $\text{G7}_{\text{Fe}_3\text{O}_4}$, $\text{G11}_{\text{MnO}_2}$ and $\text{G13}_{\text{MnO}_2}$ modified electrodes were characterized by Raman spectroscopy, before and after the chronoamperometric stability test performed during the water splitting experiments. The recorded spectra are presented in **Figures 6** and **7**. In the case of $\text{G7}_{\text{Fe}_3\text{O}_4}$ (**Figure 6**), it cannot be said that the chemical structure of the materials used to manufacture the electrode changed as a result of the test carried out during the OER investigations. The broad and intense peaks at 1354 and 1597 cm^{-1} probably belong to the conductive carbon present in the combination used to obtain the modified electrode [44], while the peaks at 354 , 492 , and 700 cm^{-1} can be attributed to the iron oxide [45].

With regard to the $\text{G11}_{\text{MnO}_2}$ and $\text{G13}_{\text{MnO}_2}$ electrodes (**Figures 7a** and **7b**), the spectra recorded after the chronoamperometric experiment are not significantly different from the initial ones, which indicates that the materials used to modify the graphite substrates did not suffer structural changes during the stability testing. In the case of $\text{G11}_{\text{MnO}_2}$, a slight broadening of the

peak at 654 cm^{-1} is observed on the spectrum obtained after the test that can be attributed to sample heating during the Raman analysis. The values at which the peaks identified for the two electrodes appear are similar to those reported in the literature for MnO_2 [46].

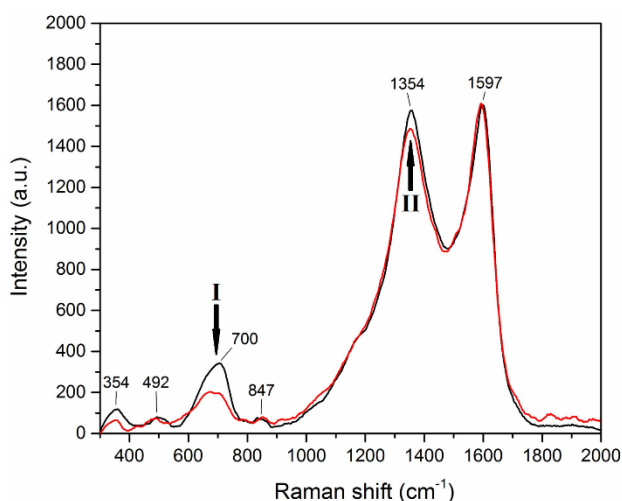


Figure 6. Raman spectra recorded on the G7_{Fe3O4} electrode before the electrochemical stability test (I) and afterwards (II)

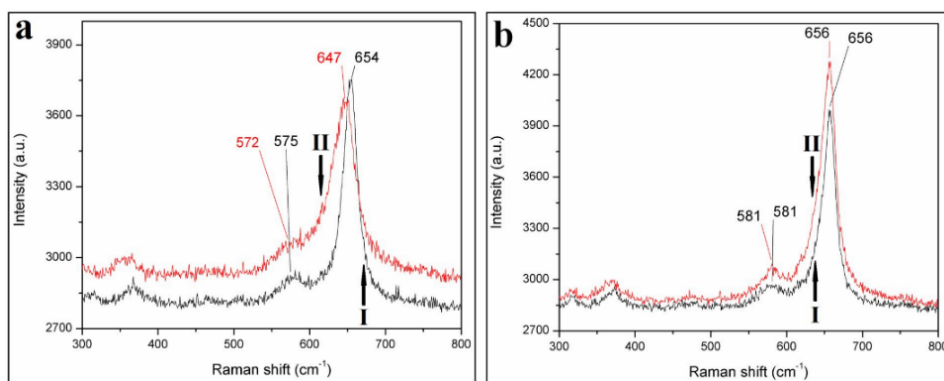


Figure 7. Raman spectra recorded on the G11_{MnO2} (a) and G13_{MnO2} (b) electrodes before the stability test (I) and afterwards (II)

CONCLUSIONS

The water splitting experiments performed in alkaline medium on graphite electrodes modified using suspensions in ethanol containing a transition metal oxide (Fe_3O_4 or MnO_2), as such or in compositions with Carbon Black and/or Nafion solution, have led to the identification of the most catalytically active samples. Out of the iron oxide-based electrodes the most performant was the one labeled G7 $_{\text{Fe}_3\text{O}_4}$ and it displayed the highest catalytic activity for both O_2 and H_2 evolution reactions. However, the electrochemical stability of this electrode under HER conditions was poor. The main problem with its OER activity is the high Tafel slope value, but its properties can be improved through an optimization process employing a more advanced modification method than drop-casting (such as laser ablation deposition), that will lead to the manufacturing of a more stable sample, having a smaller Tafel slope value.

Regarding the manganese oxide-based electrodes, the best OER activity was observed for G13 $_{\text{MnO}_2}$, while the best HER activity was displayed by G11 $_{\text{MnO}_2}$. In terms of electrochemical stability, the two electrodes were shown to be fairly stable, but an optimization process - focused on deposition method and substrate - is recommended for enhancing their catalytic activity.

EXPERIMENTAL SECTION

Materials and reagents

MnO_2 was synthesized hydrothermally from a mixture of 20 mmol KMnO_4 , 30 mmol $\text{Mn}(\text{NO}_3)_2$ and 40 mmol KOH . This mixture was obtained by dissolving each precursor in 20 mL double-distilled water and blending the solutions under continuous stirring, and was transferred into a stainless steel Teflon-lined autoclave. After sealing, the autoclave was placed in an oven at 180 °C. The thermal treatment lasted for 21 hours and was followed by a cooling stage to room temperature. The cooled reaction product was filtered, repeatedly washed with double-distilled water and afterwards with ethanol. The subsequent drying stage lasted for 4 hours at 80 °C.

The synthesis of Fe_3O_4 was also hydrothermal, using 2M NaOH solution and a mixture of $\text{FeCl}_3 \times 6\text{H}_2\text{O}$ and $\text{FeSO}_4 \times 7\text{H}_2\text{O}$ (in 1:2 molar ratio). The precursors were at first dissolved individually in 20 mL volumes of double-distilled water. The mixing took place under continuous stirring and the NaOH solution was added dropwise to the blend, also under stirring. The resulted black suspension was introduced into a stainless steel Teflon-lined

autoclave that was sealed and placed in an oven at 220 °C, for 5 hours. This stage was followed by cooling at room temperature, after which the reaction product was filtered, washed repeatedly with double-distilled water and then with ethanol, and it was subsequently dried for 4 hours at 80 °C.

The conductive substrate used in the electrode manufacturing process was spectroscopic graphite, type SW.114, from “Kablo Bratislava”, National Corporation “Electrocarbon Topolcany” Factory (Slovakia). The MnO₂- and Fe₃O₄-based compositions contained conductive carbon (Carbon Black - Vulcan XC 72 from Fuel Cell Store) and/or Nafion solution (Nafion® 117 solution of 5% concentration from Sigma-Aldrich). Nafion was used as binder to ensure better adhesion between the materials evaluated in terms of their OER and HER catalytic properties and the conductive substrate on which they were deposited. Other reagents used in the study were: KOH, KNO₃, K₃[Fe(CN)₆], 96% C₂H₅OH and (CH₃)₂CO, purchased from Sigma-Aldrich, Merck and Chimreactiv. All solutions were obtained using laboratory produced double-distilled water.

Manufacturing of the modified electrodes

Modification of the graphite support with electrocatalytic materials was performed via the drop-casting method. Specifically, by applying droplets from ethanol suspensions prepared by dispersing the MnO₂, Fe₃O₄ and the compositions containing them in 0.5 mL ethanol. After 30 minutes ultrasonication, volumes of 10 µL were prelevated from the suspensions and were applied on the graphite surfaces. This was followed by solvent evaporation at 50 °C and the resulted electrodes were kept at room temperature until their experimental use. Ethanol was employed in the obtaining of the suspensions in part because it is used for this purpose in reported studies investigating the OER and HER properties of MnO₂-based electrodes [22,24,43], but also because it led to an improved dispersion of the Carbon Black particles, considering their hydrophobic nature. **Tables 1** and **2** present the labels used to refer to the modified electrodes, as well as the compositions of the suspensions from which they were obtained.

An electrochemical assembly consisting of a glass cell equipped with three electrodes, connected to a Voltalab PGZ 402 potentiostat (Radiometer Analytical) was employed to perform the electrochemical investigations on the modified electrodes. The counter electrode was a Pt plate ($S_{\text{geom}} = 0.8 \text{ cm}^2$) and the Ag/AgCl electrode (sat. KCl) was used as reference. The unmodified graphite electrode (labeled G0) and the electrodes labeled according to **Tables 1** and **2** were each used as the working electrode ($S_{\text{geom}} = 0.28 \text{ cm}^2$).

Table 1. The labels for the Fe₃O₄-based modified electrodes and the compositions of the suspensions used to obtain them

Electrode label	Fe ₃ O ₄ powder [mg]	Carbon Black powder [mg]	Nafion solution [μL]
G1 _{Fe3O4}	2	-	-
G2 _{Fe3O4}	4	-	-
G3 _{Fe3O4}	6	-	-
G4 _{Fe3O4}	2	1	-
G5 _{Fe3O4}	4	1	-
G6 _{Fe3O4}	6	1	-
G7 _{Fe3O4}	2	2	-
G8 _{Fe3O4}	4	2	-
G9 _{Fe3O4}	6	2	-
G10 _{Fe3O4}	2	-	10
G11 _{Fe3O4}	4	-	10
G12 _{Fe3O4}	6	-	10
G13 _{Fe3O4}	2	1	10
G14 _{Fe3O4}	4	1	10
G15 _{Fe3O4}	6	1	10
G16 _{Fe3O4}	2	2	10
G17 _{Fe3O4}	4	2	10
G18 _{Fe3O4}	6	2	10

Table 2. The labels for the MnO₂-based modified electrodes and the compositions of the suspensions used to obtain them

Electrode label	MnO ₂ powder [mg]	Carbon Black powder [mg]	Nafion solution [μL]
G1 _{MnO2}	2	-	-
G2 _{MnO2}	4	-	-
G3 _{MnO2}	6	-	-
G4 _{MnO2}	2	1	-
G5 _{MnO2}	4	1	-
G6 _{MnO2}	6	1	-
G7 _{MnO2}	2	2	-
G8 _{MnO2}	4	2	-
G9 _{MnO2}	6	2	-
G10 _{MnO2}	2	-	10
G11 _{MnO2}	4	-	10
G12 _{MnO2}	6	-	10
G13 _{MnO2}	2	1	10
G14 _{MnO2}	4	1	10
G15 _{MnO2}	6	1	10
G16 _{MnO2}	2	2	10
G17 _{MnO2}	4	2	10
G18 _{MnO2}	6	2	10

The graphite supports were in the shape of rods inserted in polyethylene tubes that were sealed to them through heat treatment at 180 °C. One of the ends of each rod was polished with silicon carbide paper (grit sizes: 600, 800

and 1200, respectively) and felt, subsequently washed with water, ethanol and acetone, and dried at room temperature. During the experiments, the polished rod end was immersed into the electrolyte solution, as such or after modification with the catalytic materials, while the other end was connected to the potentiostat.

The values of the electrochemical potential (E) are expressed in terms of the reversible hydrogen electrode (RHE) using Equation (1), the values of the OER overpotential were calculated with Equation (2) [47], and those of the HER overpotential with Equation (3).

$$E_{RHE} [V] = E_{Ag/AgCl(sat. KCl)} + 0.059 \times pH + 0.197 \quad (1)$$

$$\eta_{O_2} [V] = E_{RHE} - 1.23 \quad (2)$$

$$\eta_{H_2} [V] = |E_{RHE}| \quad (3)$$

Where: E_{RHE} = the potential of the Reversible Hydrogen Electrode [V], $E_{Ag/AgCl(sat. KCl)}$ = the potential of the Ag/AgCl (sat. KCl) electrode [V], η_{O_2} and η_{H_2} are the OER and HER overpotentials [V].

The current density values (i) referred to in the study are geometric current densities, unless otherwise specified. The OER and HER investigations were performed by recording iR-corrected linear sweep voltammograms (LSVs), at $v = 5$ mV/s, in 0.1M and 1M KOH electrolyte solutions. For the HER measurements the electrolyte solutions were deaerated with N_2 .

The electroactive surface area (EASA) of the most catalytically active electrodes was estimated using Equation (4) - the Randles-Sevcik equation [48,49] - together with cyclic voltammetry data obtained at different scan rates in 1M KNO_3 solution, in the absence and presence of 4 mM $K_3[Fe(CN)_6]$.

$$I_p = (2.69 \times 10^5) \times n^{3/2} \times A \times D^{1/2} \times C \times v^{1/2} \quad (4)$$

Where: I_p = peak current [A]; n = number of electrons involved in the redox process at $T = 298$ K; A = working electrode surface [cm^2]; D = diffusion coefficient of the electroactive species [cm^2/s]; C = concentration of the electroactive species [M] and v = scan rate [V/s]. For the ferrocyanide/ferricyanide redox couple $n = 1$ and the theoretical value of $D = 6.7 \times 10^{-6}$ cm^2/s [50].

Raman spectroscopy analysis

The most catalytically performant electrodes identified during the OER and HER studies were analyzed by Raman spectroscopy, using a MultiView-2000 system from Nanonics Imaging Ltd. (Israel), equipped with a

Shamrock 500i spectrograph from ANDOR (UK). The analyses were performed at room temperature, with a 50x objective, using as excitation source a laser radiation with $\lambda = 514.5$ nm and an exposure time of 20s.

ACKNOWLEDGMENTS

This work was financed by the National Program NUCLEU, Project Code PN 19 22 01 01, Contract No. 40N/2019.

REFERENCES

1. M. F. Sapountzi; M. J. Gracia; C. J. Weststrate; O. A. H. Fredriksson; J. W. Niemantsverdriet; *Prog. Energy Combust. Sci.*, **2017**, *58*, 1-35.
2. S. Wang; A. Lu; C.-J. Zhong; *Nano Converg.*, **2021**, *8*, 1-23.
3. N. Dubouis; A. Grimaud; *Chem. Sci.*, **2019**, *10*, 9165-9181.
4. L. Li; P. Wang; Q. Shao; X. Huang; *Chem. Soc. Rev.*, **2020**, *49*, 3072–3106.
5. D. Yao; L. Gu; B. Zuo; S. Weng; S. Deng; W. Hao; *Nanoscale*, **2021**, *13*, 10624-1064.
6. Q. Tang; D. Jiang; *ACS Catal.*, **2016**, *6*, 4953–4961.
7. M. I. James; *J. Power Sources*, **2016**, *333*, 213-236.
8. R. L. Doyle; M. E. G. Lyons; *Phys. Chem. Chem. Phys.*, **2013**, *15*, 5224-5237.
9. S. K. Ghosh; H. Rahaman; Noble metal–manganese oxide hybrid nanocatalysts, in *Noble Metal-Metal Oxide Hybrid Nanoparticles. Fundamentals and Applications. Micro and Nano Technologies*, S. Mohapatra, T. A. Nguyen, P. Nguyen-Tri Eds.; Woodhead Publishing, Sawston, UK, **2019**, Chapter 16, pp. 313-340.
10. I. Concina; Z. H. Ibupoto; A. Vomiero; *Adv. Energy Mater.*, **2017**, *7*, 1-29.
11. M. Chhetri; S. Sultan; C. N. R. Rao; *PNAS*, **2017**, *114*, 8986-8990.
12. P. W. Menezes; C. Panda; S. Loos; F. Bunschei-Bruns; C. Walter; M. Schwarze; X. Deng; H. Dau; M. Driess; *Energy Environ. Sci.*, **2018**, *11*, 1287-1298.
13. W. Li; D. Xiong; X. Gao; L. Liu; *Chem. Commun.*, **2019**, *55*, 8744-8763.
14. T. Priamushko; R. Guillet-Nicolas; F. Kleitz; *Inorganics*, **2019**, *7*, 1-21.
15. P. Xiao; W. Chen; X. Wang; *Adv. Energy Mater.*, **2015**, *5*, 1-13.
16. M. Zeng; Y. Li; *J. Mater. Chem. A*, **2015**, *3*, 14942-14962.
17. J. Li; J. Li; X. Zhou; Z. Xia; W. Gao; Y. Ma; Y. Qu; *ACS Appl. Mater. Interfaces*, **2016**, *8*, 10826–10834.
18. X. Wang; W. Li; D. Xiong; D.Y. Petrovykh; L. Liu; *Adv. Funct. Mater.*, **2016**, *26*, 4067–4077.
19. S. Ghosh; R. N. Basu; *Nanoscale*, **2018**, *10*, 11241-11280.
20. J. Melder; P. Bogdanoff; I. Zaharieva; S. Fiechter; H. Dau; P. Kurz; *Z. fur Phys. Chem.*, **2020**, *234*, 925–978.

21. Y. Meng; W. Song; H. Huang; Z. Ren; S.-Y. Chen; S.L. Suib; *J. Am. Chem. Soc.*, **2014**, *136*, 11452–11464.
22. R. Pokhrel; M. K. Goetz; S. E. Shaner; X. Wu; S. Stahl; *J. Am. Chem. Soc.*, **2015**, *137*, 8384–8387.
23. F. Speck; P. Santori; F. Jaouen; S. Cherevko; *J. Phys. Chem.*, **2019**, *123*, 25267–25277.
24. Y. Zhao; C. Chang; F. Teng; Y. Zhao; G. Chen; R. Shi; G. I. N. Waterhouse; W. Huang; T. Zhang; *Adv. Energy Mater.*, **2017**, *7*, 1-7.
25. M. Mullner; M. Riva; F. Kraushofer; M. Schmid; G. S. Parkinson; S. F. L. Mertens; U. Diebold; *J. Phys. Chem.*, **2019**, *123*, 8304–8311.
26. R. Phul; M. A. M. Khan; M. Sardar; J. Ahmed; T. Ahmad; *Crystals*, **2020**, *10*, 1-14.
27. R. H. Tammam; A. M. Fekry; M. M. Saleh; *Korean J. Chem. Eng.*, **2019**, *36*, 1932-1939.
28. M. B. Askari; A. Beheshti-Marnani; M. Seifi; S. M. Rozatia; P. Salarizadeh; *J. Colloid Interface Sci.*, **2019**, *537*, 186-196.
29. S. Han; S. Liu; S. Yin; L. Chen; Z. He; *Electrochim. Acta*, **2016**, *210*, 942-949.
30. F. Mirabella; M. Müllner; T. Touzalin; M. Riva; Zdenek Jakub; F. Kraushofer; Michael Schmid; M.T.M. Koper; G.S. Parkinson; U. Diebold; *Electrochim. Acta*, **2021**, *389*, 1-11.
31. J. Yang; Q. Shao; B. Huang; M. Sun; X. Huang; *iScience*, **2019**, *11*, 492-504.
32. V. Mani; S. Anantharaj; S. Mishra; N. Kalaiselvi; S. Kundu; *Catal. Sci. Technol.*, **2017**, *7*, 5092–5104.
33. I. Barauskien; E. Valatka; *Mater. Renew. Sustain. Energy*, **2018**, *7*, 1-10.
34. I. Sebarchievici; B.-O. Taranu; M. Birdeanu; S. F. Rus; E. Fagadar-Cosma; *Appl. Surf. Sci.*, **2016**, *39*, 131-140.
35. B.-O. Taranu; M. G. Ivanovici; P. Svera; P. Vlazan; P. Sfirloaga; M. Poienar; *J. Alloys Compd.*, **2020**, *848*, 1-11.
36. Z.-Y. Wu; B.-C. Hu; P. Wu; H.-W. Liang; Z.-L. Yu; Y. Lin; Y.-R. Zheng; Z. Li; S.-H. Yu; *NPG Asia Mater.*, **2016**, *8*, 1-8.
37. X. Wang; YV Kolen'ko; X.-Q. Bao; K. Kovnir; L. Liu; *Angew. Chem. Int. Ed.*, **2015**, *54*, 8188–8192.
38. Z. Liu; H. Tan; D. Liu; X. Liu; J. Xin; J. Xie; M. Zhao; L. Song; L. Dai; H. Liu; *Adv. Sci.*, **2019**, *6*, 1-11.
39. H. Wang; H.-W. Lee; Y. Deng; Z. Lu; P.-C. Hsu; Y. Liu; D. Lin; Y. Cui; *Nat. Comm.*, **2015**, *6*, 1-8.
40. Y. Li; H. Wang; L. Xie; Y. Liang; G. Hong; H. Dai; *J. Am. Chem. Soc.*, **2011**, *133*, 7296–7299.
41. A. Lahiri; G. Li; F. Endres; *J. Solid State Electrochem.*, **2020**, *24*, 2763–2771.
42. I. Boshnakova; E. Lefterova; E. Slavcheva; *Int. J. Hydrog. Energy*, **2018**, *43*, 16897-16904.
43. H. Begum; M. S. Ahmed; S. Jeon; *Electrochim. Acta*, **2019**, *296*, 235-242.
44. R. Hatel; S. E. Majdoub; A. Bakour; M. Khenfouch; M. Baitoul; *IOP Conf. Series: Journal of Physics: Conf. Series*, **2018**, *1081*, 1-7.
45. C. Guo; Y. Hu; H. Qian; J. Ning; S. Xu; *Mater. Charact.*, **2011**, *62*, 148-151.

46. B. Yin; S. Zhang; H. Jiang; F. Qu; X. Wu; *J. Mater. Chem. A*, **2015**, *3*, 5722-5729.
47. Z. Zhao; H. Wu; H. He; X. Xu; Y. Jin; *J. Mater. Chem. A*, **2015**, *3*, 7179-7186.
48. A. Baciú; A. Remes; E. Ilinoiu; F. Manea; S.J. Picken; J. Schoonman; *Environm. Eng. Manag. J.*, **2012**, *11*, 239-246.
49. E.C. Ilinoiu; F. Manea; P.A. Serra; R. Pode; *Sensors*, **2013**, *13*, 7296-7307.
50. M. Yang; Y. Yang; Y. Liu; G. Shen; R. Yu; *Biosens. Bioelectron.*, **2006**, *21*, 1125–1131.

